Block Copolymer Membrane

DOI: 10.1002/anie.201404491

Self-Assembled Isoporous Block Copolymer Membranes with Tuned Pore Sizes**

*Haizhou Yu, Xiaoyan Qiu, Suzana P. Nunes, and Klaus-Viktor Peinemann**

Abstract: *The combination of nonsolvent-induced phase separation and the self-assembly of block copolymers can lead to asymmetric membranes with a thin highly ordered isoporous skin layer. The effective pore size of such membranes is usually larger than 15 nm. We reduced the pore size of these membranes by electroless gold deposition. We demonstrate that the pore sizes can be controlled precisely between 3 and 20 nm leading to a tunable sharp size discrimination in filtration processes. Besides fractionation of nanoparticles and biomaterials, controlled drug delivery is an attractive potential application.*

Newly developed membrane separation processes offer substantial economic, environmental (lower energy consumption), and safety benefits in comparison to conventional resin-based chromatography which is time-consuming.[1,2] Micro/nanofabricated membranes with various pore sizes, lengths, morphologies, and densities have been synthesized from diverse inorganic, organic, and composite materials.[3–7] Although a number of methods have been developed for producing porous materials,[8–10] it still remains a great challenge to produce porous membranes with an ordered periodic structure, high porosity, and precisely controlled pore sizes. Yang et al. developed a new drug delivery device by thermally depositing gold on a spin-coated block copolymer thin film.[11] Controlled release of protein drugs by single-file diffusion (SFD) was successfully demonstrated by controlling the pore size. However, scale-up might be a challenge considering the fabrication process. Chun et al. reduced the pore size of a track-etched polycarbonate membrane by electroless gold deposition.[12] The surface was further modified with self-assembled monolayers (SAMs) of functionalized thiols ($HSC_{10}H_{20}COOH$) to separate two similar-sized proteins. Although they achieved a higher separation selectivity, the complicated procedure and low pore density (6 pores μm^{-2}) could limit the use of the membranes.

[*] Dr. H. Z. Yu,[+] Dr. X. Y. Qiu,[+] Prof. K. V. Peinemann
Advanced Membranes and Porous Materials Center
4700 King Abdullah University of Science and Technology (KAUST)
Thuwal 23955-6900 (Kingdom of Saudi Arabia)
E-mail: klausviktor.peinemann@kaust.edu.sa
Prof. S. P. Nunes
Water Desalination and Reuse Center (KAUST)
Thuwal 23955-6900 (Kingdom of Saudi Arabia)
[+] These authors contributed equally to this work.
[**] The work was supported by the KAUST Seed-Fund Project "Isoporous Membranes".
Supporting information for this article is available on the WWW under http://dx.doi.org/10.1002/anie.201404491.

Previously, our group has reported the preparation of an integral asymmetric membrane through a very fast one-step procedure by combining the self-assembly of an amphiphilic block copolymer (PS-*b*-P4VP) and nonsolvent-induced phase separation.[13–16] The structure comprises a top thin layer exhibiting highly ordered cylindrical channels of uniform pore size perpendicular to the surface at extremely high density and a non-ordered sponge-like layer beneath. After further modification this membrane has been reported for the first time not only for size-based protein separation, but also for separations of similarly sized proteins.[17] Here, we report the control of the pore size of self-assembled PS-*b*-P4VP block copolymer membranes by an electroless gold deposition method. The gold-coated membranes exhibit sharp cutoffs that can be tuned between ca. 3.0 and 20.0 nm. We envision that these membranes with tunable pore sizes will thus possess attributes useful for applications in nanoparticle separations and long-term controlled drug delivery.

Scheme 1 shows the electroless gold deposition process for the fabrication of isoporous block copolymer membranes. An integral asymmetric membrane from polystyrene-*b*-poly(4-vinylpyridine) (PS-*b*-P4VP, 175 000-*b*-65 000 $g\,mol^{-1}$) was fabricated using an innovative and simple method.[13] The polymer-rich phase (PS blocks) forms the porous matrix, whereas the polymer-poor phase (P4VP blocks) gives rise to the pores (Scheme 1 B). The lone electron pair on nitrogen of P4VP acts as a strong ligand for coordination with metal ions such as Au^{3+} (Scheme 1 A).[15] The gold layer was deposited as a result of a two-step redox reaction on the walls of the nanopores. By controlling the concentration of $HAuCl_4 \cdot 3H_2O$

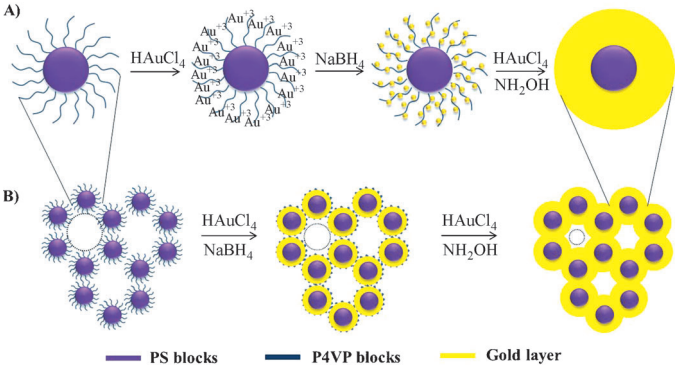

Scheme 1. The preparation of a block copolymer membrane with controlled pore sizes through electroless gold deposition: A) gold decoration on a single micelle and B) pore evolution of the membrane with gold deposition.

in the first step, we could precisely control the thickness of the gold layer as well as the pore size of the membrane. Although P4VP can coordinate with other metal ions, Au was chosen because of its good biocompatibility and excellent adhesion to the membrane.[18] In addition, the gold deposition reduced protein fouling of the block copolymer membrane in the present work. Figure 1 shows the scanning electron microscopy (SEM) images of the block copolymer membranes after the first step of gold deposition. The plain membrane is characterized by cylindrical isopores, which after immersion in a solution of 0.01 wt% $HAuCl_4{\cdot}3H_2O$ have a diameter of ca. 25.6 nm (measured from SEM images), as shown in Figure 1 A,D. The pore size decreased to ca. 10 nm when the concentration of $HAuCl_4{\cdot}3H_2O$ was increased from 0.01 wt% to 0.1 wt% (Figure 1 B,E). Figures 1 C and 1 F show membranes first immersed in a solution of 1 wt% $HAuCl_4{\cdot}3H_2O$ followed by the second step to complete the electroless plating.[19–21] In the second step, the membrane with the precoated gold layer was immersed in a mixture of $HAuCl_4{\cdot}3H_2O$ (0.01 wt%) and NH_4OH (4 mM) for 30 min. The precoated gold layer serves as the nucleation site for electroless metal deposition. The NH_4OH addition causes a rapid increase in the pH of the solution, resulting in the preferential deposition onto the existing gold surfaces rather than the nucleation of additional gold particles.[22] An indication of the decreasing pore size with the increase of the $HAuCl_4{\cdot}3H_2O$ concentration is given by the color change shown in Figure 1 G. Here, the area of an as-produced membrane was more than 50 cm^2, which made it easy to handle and use. The final membrane discs for testing had a diameter of 2.2 cm.

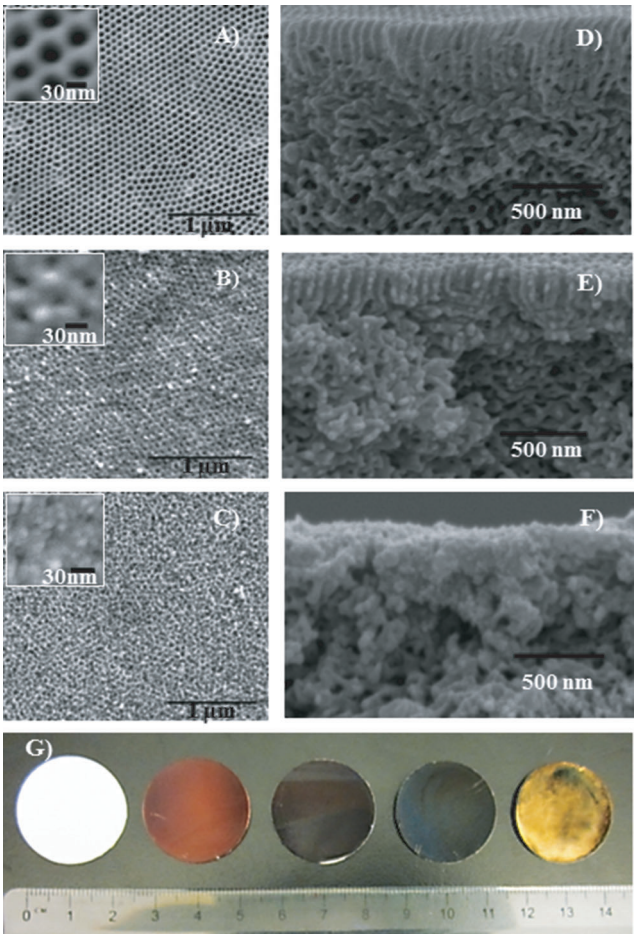

Figure 1. SEM images show the surfaces (A–C) and cross-sections (D–F) of three typical membranes with different pore sizes after gold deposition, performed by treatment with $HAuCl_4{\cdot}3H_2O$ solutions of different concentrations: A,D) 0.01 wt%, B,E) 0.1 wt%, C,F) 1.0 wt%. The membranes in (C) and (F) were then immersed in a mixture of $HAuCl_4{\cdot}3H_2O$ (0.01 wt%) and NH_4OH (4 mM) to increase the thickness of the gold layer. The corresponding effective pore sizes were 18.8 nm, 10.1 nm, and 3.0 nm, respectively. G) Discs showing concentration-dependent gold coating; left to right: untreated membrane; membranes treated with 0.01 wt%, 0.05 wt%, 0.1 wt%, and 1.0 wt% $HAuCl_4{\cdot}3H_2O$. The ruler shown below the discs is marked in centimeters.

The membrane water flux as a function of $HAuCl_4{\cdot}3H_2O$ concentration is shown in Figure 2 (blue curve). Due to the high porosity (ca. 2.2×10^{14} pores per square meter from SEM image) and the thin top layer (ca. 100 nm), the water flux through the membrane was more than 3000 $L\,m^{-2}h^{-1}bar^{-1}$ without gold deposition, which was more than one order of magnitude higher than the water fluxes of commercially available membranes with comparable pore sizes. Under the assumption that the main flow resistance was in the 100 nm thick ordered top layer,[17] the Hagen–Poiseuille law can be applied to give an estimation of the effective pore size corresponding to the measured water flux through the membrane:

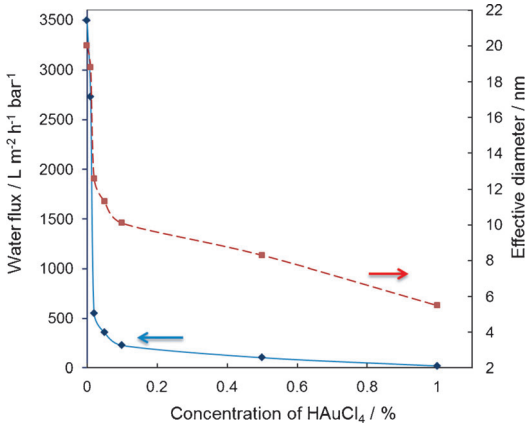

Figure 2. Water flux (blue curve) and effective pore diameter (red) of the nanoporous membrane as a function of the concentration of $HAuCl_4{\cdot}3H_2O$, measured at 1.38 bar feed pressure.

$$dv/dt = (\pi R^4 \Delta p)/(8\eta L)$$

in which R is the pore radius, ΔP is the pressure drop across the membrane, η is the water viscosity (8.9×10^{-4} $Pa\,s^{-1}$ at 25 °C), and L is the length of the selective pores. The effective pore diameter of the membrane was estimated to be approximately 20 nm without gold deposition.

The red curve in Figure 2 exhibits the effective pore diameters estimated by the Hagen–Poiseuille equation. Obviously, both the flux and the effective pore diameter decreased when the concentration of $HAuCl_4 \cdot 3H_2O$ was increased. The effective pore diameter after the second step of gold deposition was estimated to be less than 3.5 nm (not shown in Figure 2); this was subsequently confirmed by the nanoparticle separation experiments. The water flux of the membrane as well as the effective pore diameter became less pH-responsive after gold deposition (Figure S1), which could be advantageous for applications under different pH conditions, requiring constant flux.

The performance of the membranes with different pore sizes after the gold deposition was evaluated by filtering gold nanoparticles with sizes ranging from 3.5 to 35 nm in diameter (Figure S2). The membranes (diameter 2.2 cm) were tested in a dead-end Amicon cell at a pressure of 1.38 bar, by starting with a feed volume of 6 mL and collecting 3 mL of permeate. Absorbance values in the feed and filtrate were measured to determine concentrations, and these were normalized to calculate sieving coefficients. Results show that each membrane after gold deposition exhibited a sharp cutoff with negligible transport of large particles and significant permeation (40–90%) of the small particles (Figure 3A). The cutoffs of the membranes match well with the estimated effective pore diameters in Figure 2. Most notably, membrane (d) with an effective pore diameter of ca. 5.5 nm (Figure 2) allowed more than 85% permeation of 3.5 nm particles and blocked the larger 6.5 nm particles (Figure 3A). Membrane (e) after the second step of gold deposition exhibited a cutoff smaller than 3.5 nm (Figure 3A).

The uniform pores after gold deposition enabled the separation of mixtures of nanoparticles with similar sizes. As shown in Figure 3B, when a mixture of ca. 2.5–10 nm nanoparticles is filtered, the system largely recovers the light absorbance corresponding to smaller nanoparticles with a peak shift from ca. 520 nm to ca. 510 nm. The inset in Figure 3B indicates the color change of the feed solution, which is a direct demonstration of the rejection of the larger particles by membrane (e). As shown by the TEM images and DLS results in Figure 3C, the feed solution contained gold nanoparticles with a broad size distribution in the range of ca. 2.5–10 nm. However, the TEM image and DLS analysis of the filtrate (Figure 3D) indicated that only small nanoparticles (< 3.0 nm) could pass through membrane (e), which agrees well with Figure 3A. We also switched from the simple pressure cell to a cell with centrifuge-generated pressure. Gold nanoparticles were filtered in the centrifuge tubes, which were equipped with block copolymer membranes (diameter 0.8 cm). Results showed that small particles were forced through the membrane, leaving the larger ones in the retentate at a centrifuge pressure of 14000 rpm without mechanical failure (Figure 3E). This process could be completed in several seconds, enhancing the separation efficiency.

The pore size and pore size distribution of the membrane was also estimated by Brunauer–Emmett–Teller (BET) analysis. The BET result was calculated from N_2 adsorption isotherms using the Barrett–Joyner–Halenda (BJH) method. The narrow pore size distribution (Figure S3a) is consistent

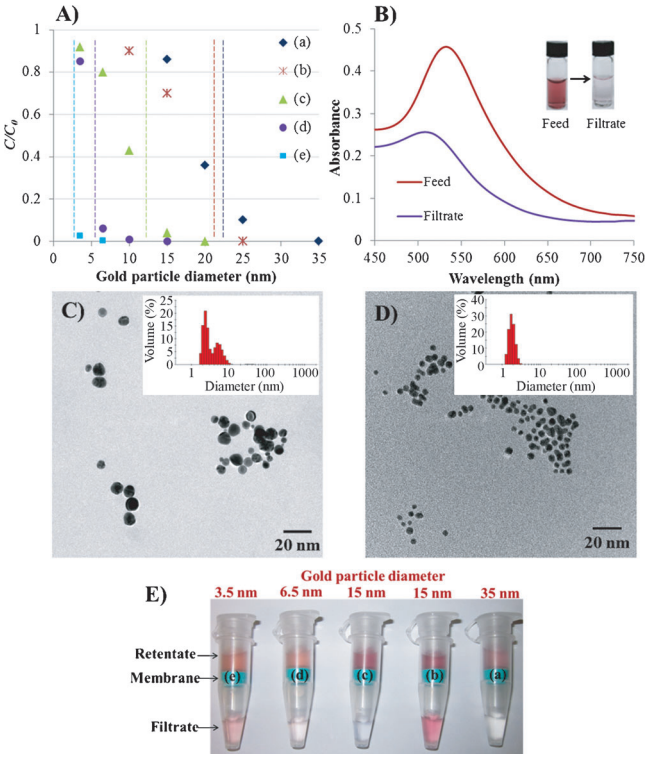

Figure 3. A) Filtration of gold nanoparticles with sizes of 3.5–35 nm. Gold nanoparticles were filtered through five different membranes after gold deposition with different concentrations of $HAuCl_4 \cdot 3H_2O$: membrane (a) 0%, (b) 0.01 wt%, (c) 0.1 wt%, (d,e) 1.0 wt%; membrane (e) was analogous to (d), but was submitted to the second step of electroless deposition. The plot shows the ratio of concentrations in the permeate (C) and feed solutions (C_0) as a function of nanoparticle size. Dashed lines are the apparent cutoffs of the membranes. B) UV/Vis spectra of the feed solution containing a size distribution of ca. 2.5–10 nm gold particles, and the filtrate solution after separation by membrane (e). C and D) TEM images of the feed and filtrate solutions, respectively. Insets are the corresponding DLS results. E) Images of the retentate and filtrate solutions from gold particle separations with five different membranes (a–e) in the centrifuge tube.

with the sharp cutoff of the membrane and is much sharper than that of a commercial PAN membrane with a similar pore size (Figure S3b).

Considering that gold was deposited on the entire membrane (Figure 1 and Figure S4) and the pores after gold deposition are size-tunable and biocompatible, the membranes could serve as a synthetic drug delivery system. Controlled and long-term protein drug delivery has been considered as one of the most promising biomedical applications of nanotechnology.[23] A wide range of materials and devices have been developed for the delivery of protein drugs in a controlled manner within a therapeutic range.[24,25] However, controlled-release depot systems for protein drugs lasting for longer than a week are still a challenge.[11] In the present work, three isoporous membranes (diameter 2.2 cm) with different pore diameters after gold deposition, i.e., 12.6 nm, 10.1 nm, and 8.3 nm, were examined for the in vitro delivery of bovine serum albumin (BSA) with a molecular weight of 67 kDa and a hydrodynamic diameter of ca. 6.8 nm.

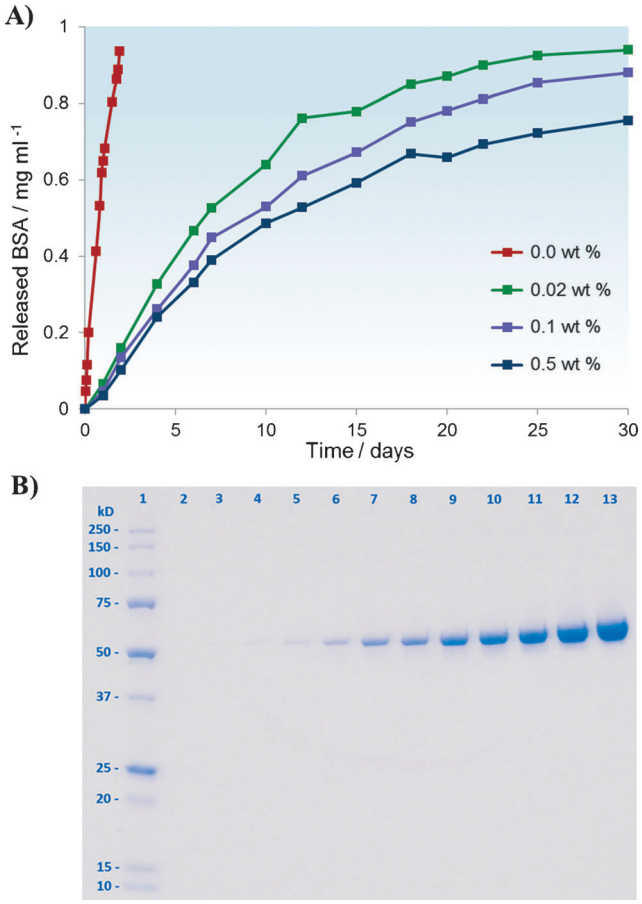

Figure 4. A) In vitro release profile of BSA through the untreated membrane (red squares) and the membranes after gold coating with different concentrations of $HAuCl_4 \cdot 3\,H_2O$. B) The results of SDS-PAGE analysis of in vitro released BSA over 30 days. Lane 1: 5 μL protein molecular weight standards; Lane 2: blank; Lanes 3–12: 10 μL released protein samples collected after 1, 4, 6, 10, 12, 15, 18, 22, 25, and 30 days, respectively; Lane 13: 10 μL initial stock solution of BSA (2 mg mL^{-1}).

An untreated membrane with an effective pore diameter of ca. 20 nm was also examined for comparison.

Figure 4A shows the in vitro release profile of BSA through these membranes over up to one month. A sharp curve (red), i.e., a fast release within one day, was observed using the untreated membrane, which is not ideal for long-term drug delivery. However, the experiment showed that the release rate is decreased and could be controlled by adjusting the pore size through electroless gold deposition. A constant release of BSA based on single-file diffusion (SFD),[11,26,27] was observed during the first five days followed by a slight decrease over the next 10 days (Figure 4A). This is known to be the most appropriate performance expected for a long-term controlled delivery of protein drugs. After 10 days, a slowdown in the release rate occurred, which resulted from the decrease of the concentration difference between the two chambers. The results are quite reasonable, because the SFD of BSA is possible when the diameter of the membrane pores is less than twice the hydrodynamic diameter of the protein (ca. 13.6 nm). In this situation, two or more protein molecules cannot pass simultaneously through the pores. 1D SDS-PAGE analysis was carried out to confirm that the released protein drug is intact and no denaturation has occurred. The BSA released even after 30 days was detected at the same position with the molecular weight unchanged as shown in Figure 4B, indicating that BSA remained its original active structure after release.

The protein single-file diffusion described above was also observed by Yang et al.[11] They also tuned the pore size of self-assembled block copolymer membranes by gold deposition. The main advance of our work is the simple membrane preparation method and the drastically reduced manufacturing time. We prepared our membrane by a phase-separation process and could avoid spin-coating, long annealing, etching, and tedious membrane transfer to a porous support. Yang et al. applied thermal gold evaporation under high vacuum; we used a simple electroless gold plating in solution. Our shorter single-file diffusion time (30 days versus 60 days) is just a consequence of a lower starting concentration of BSA. Details are given in the Supporting Information (Figure S6).

In addition to reducing the pore size, the gold deposition appeared to reduce protein fouling to the block copolymer membrane. SEM images show a "clean" membrane before exposure to the protein solution (Figure S5A) and another membrane without gold deposition after the protein diffusion experiment (Figure S5B) with a reduced effective pore size due to fouling. Despite the extended contact time of the membranes with the protein drugs at a high initial concentration of 2 mg mL^{-1}, protein aggregation and membrane fouling were not observed on the gold-coated membranes (Figure S5C).

In summary, PS-*b*-P4VP block copolymer membranes with ordered nanopores and a high porosity were successfully synthesized. The pore sizes were precisely controlled between ca. 3 and 20 nm by electroless gold deposition. The membrane manufacturing process described here is simple and can be completed in less than one hour (no long-time annealing, no etching, no transfer to a porous support, simple gold deposition process). This manufacturing time is one to two orders of magnitude shorter than previously published processes. The sharp size discrimination, facile and scalable fabrication process, and biocompatible characteristics of the gold-coated block copolymer membranes suggest their potential uses in the purification of nanoparticles and biomaterials as well as in drug delivery.

Received: April 20, 2014
Revised: June 14, 2014
Published online: July 23, 2014

Keywords: block copolymers · drug release · gold deposition · membranes · self-assembly

[1] R. M. de Vos, H. Verweij, *Science* **1998**, *279*, 1710–1711.
[2] K. Li, *Ceramic Membranes for Separation and Reaction*, Wiley, Chichester, **2007**, Chap. 1.
[3] C. C. Striemer, T. R. Gaborski, J. L. McGrath, P. M. Fauchet, *Nature* **2007**, *445*, 749–753.

[4] R. C. Furneaux, W. R. Rigby, A. P. Davidson, *Nature* **1989**, *337*, 147 – 149.
[5] L. Li, X. Shen, S. W. Hong, R. C. Hayward, T. P. Russell, *Angew. Chem.* **2012**, *124*, 4165 – 4170; *Angew. Chem. Int. Ed.* **2012**, *51*, 4089 – 4094.
[6] L. Li, L. Schulte, L. D. Clausen, K. M. Hansen, G. E. Jonsson, S. Ndoni, *ACS Nano* **2011**, *5*, 7754 – 7766.
[7] G. Liu, J. Ding, S. Stewart, *Angew. Chem.* **1999**, *111*, 884 – 887; *Angew. Chem. Int. Ed.* **1999**, *38*, 835 – 838.
[8] D. H. Pearson, R. J. Tonucci, *Science* **1995**, *270*, 68 – 70.
[9] P. van Rijn, M. Tutur, C. Kathrein, L. Zhu, M. Wessling, U. Schwaneberg, A. Boeker, *Chem. Soc. Rev.* **2013**, *42*, 6578 – 6592.
[10] A. Imhof, D. J. Pine, *Nature* **1997**, *389*, 948 – 951.
[11] S. Y. Yang, J. A. Yang, E. S. Kim, G. Jeon, E. J. Oh, K. Y. Choi, S. K. Hahn, J. K. Kim, *ACS Nano* **2010**, *4*, 3817 – 3822.
[12] K. Y. Chun, P. Stroeve, *Langmuir* **2002**, *18*, 4653 – 4658.
[13] K.-V. Peinemann, V. Abetz, P. F. W. Simon, *Nat. Mater.* **2007**, *6*, 992 – 996.
[14] S. P. Nunes, A. R. Behzad, B. Hooghan, R. Sougrat, M. Karunakaran, N. Pradeep, K.-V. Peinemann, *ASC Nano* **2011**, *5*, 3516 – 3522.
[15] S. P. Nunes, R. Sougrat, B. Hooghan, D. H. Anjum, A. R. Behzad, L. Zhao, N. Pradeep, I. Pinnay, U. Vainio, K.-V. Peinemann, *Macromolecules* **2010**, *43*, 8079 – 8085.
[16] D. S. Marques, U. Vainio, N. M. Chaparro, V. M. Calo, A. R. Bezahd, J. W. Pitera, K.-V. Peinemann, S. P. Nunes, *Soft Matter* **2013**, *9*, 5557 – 5564.
[17] X. Qiu, H. Yu, K. Madhavan, N. Pradeep, S. P. Nunes, K.-V. Peinemann, *ACS Nano* **2013**, *7*, 768 – 776.
[18] J. J. T. Santini, M. J. Cima, R. Langer, *Nature* **1999**, *397*, 335 – 338.
[19] K. R. Brown, M. J. Natan, *Langmuir* **1998**, *14*, 726 – 728.
[20] T. Ji, V. G. Lirtsman, Y. Avny, D. Davidov, *Adv. Mater.* **2001**, *13*, 1253 – 1256.
[21] J. Zhu, W. Jiang, *Mater. Chem. Phys.* **2007**, *101*, 56 – 62.
[22] J. B. Jackson, N. J. Halas, *J. Phys. Chem. B* **2001**, *105*, 2743 – 2746.
[23] S. D. Putney, P. A. Burke, *Nat. Biotechnol.* **1998**, *16*, 153 – 157.
[24] K. Fu, A. M. Klibanov, R. Langer, *Nat. Biotechnol.* **2000**, *18*, 24 – 25.
[25] M. van de Weert, W. E. Hennink, W. Jiskoot, *Pharm. Res.* **2000**, *17*, 1159 – 1167.
[26] V. Kukla, J. Kornatowski, D. Demuth, I. Girnus, H. Pfeifer, L. V. C. Rees, S. Schunk, K. K. Unger, J. Karge, *Science* **1996**, *272*, 702 – 704.
[27] Q.-H. Wei, C. Bechinger, P. Leiderer, *Science* **2000**, *287*, 625 – 627.

